Chemical Engineering Journal 353 (2018) 126–137

Contents lists available at ScienceDirect

Chemical Engineering Journal

journal homepage: www.elsevier.com/locate/cej

One-step synthesis of Co-doped UiO-66 nanoparticle with enhanced removal efficiency of tetracycline: Simultaneous adsorption and photocatalysis

Jiao Cao[a,b], Zhao-hui Yang[a,b,*], Wei-ping Xiong[a,b], Yao-yu Zhou[c], Yan-rong Peng[a,b], Xin Li[a,b], Cheng-yun Zhou[a,b], Rui Xu[a,b], Yan-ru Zhang[a,b]

[a] College of Environmental Science and Engineering, Hunan University, Changsha 410082, PR China
[b] Key Laboratory of Environmental Biology and Pollution Control (Hunan University), Ministry of Education, Changsha 410082, PR China
[c] College of Resources and Environment, Hunan Agricultural University, Changsha 410128, PR China

HIGHLIGHTS

- Bifunctional Co-doped UiO-66 nanoparticle was synthesized by a one-step method.
- Effects of tetracycline on adsorption capacity were investigated.
- Mechanisms and tetracycline intermediates of photodegradation was described.
- Tetracycline in real samples were removed efficiently.

GRAPHICAL ABSTRACT

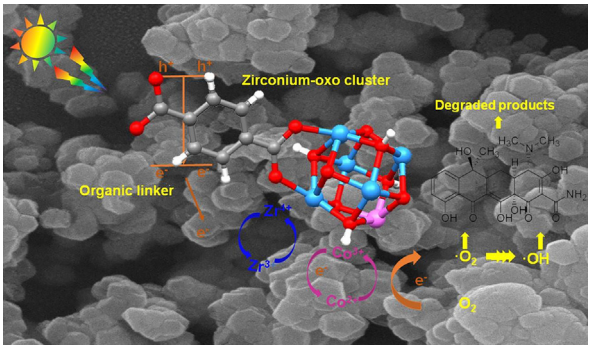

ARTICLE INFO

Keywords:
Metal-organic frameworks
Co-doped
Photocatalysis
Adsorption
Tetracycline

ABSTRACT

In this study, a novel recyclable Co-doped UiO-66 nanoparticle was synthesized by a one-step solvothermal method. A high adsorption capacity of 224.1 mg g^{-1} was obtained by the CoUiO-1 nanoparticle, then the adsorbed tetracycline (TC) molecules could be removed more than 94% of initial concentration under simulative sunlight irradiation. The adsorptive ability and photocatalytic performance of CoUiO-1 nanoparticle were about 7.6 and 6.9 times higher than the pristine UiO-66, respectively. The adsorption capacity of CoUiO-1 nanoparticle was sensitive to adsorbent dosage, coexisting ions, solution pH values and initial TC concentrations. Pseudo-second-order and Freundlich models fitted well with the adsorption process. Thermodynamic study indicated the TC adsorption on CoUiO-1 nanoparticle was a spontaneous and exothermic process. TC photodegradation experiment showed that the Co-doped modification expanded light absorption and facilitated charge separation of UiO-66, which was beneficial to enhance photocatalytic performance. The mechanism of TC photodegradation by Co-doped UiO-66 nanoparticle was investigated. Moreover, a plausible degradation pathway for TC was proposed. The high removal efficiencies of CoUiO-1 nanoparticle were obtained towards real samples including tap water, river water and pharmaceutical wastewater. Therefore, the novel Co-doped MOFs photocatalytic adsorbent showed great potential in wastewater treatment.

* Corresponding author at: College of Environmental Science and Engineering, Hunan University, Changsha, Hunan 410082, PR China.
E-mail address: yzh@hnu.edu.cn (Z.-h. Yang).

https://doi.org/10.1016/j.cej.2018.07.060
Received 10 March 2018; Received in revised form 19 June 2018; Accepted 8 July 2018
Available online 09 July 2018
1385-8947/

1. Introduction

Antibiotics, a kind of significant pharmaceutical ingredients, have been widely used in human and veterinary medicine [1,2]. It has been reported that the antibiotics concentrations in untreated domestic wastewater range between 100 ng L^{-1} and 6 μg L^{-1}, while the concentrations in pharmaceutical and hospital wastewater can reach up to 100–500 mg L^{-1} [3]. Antibiotic pollution in aqueous environment is becoming a worldwide environmental issue for their solubility, persistence and high toxicity [4,5]. Tetracycline (TC) antibiotic is widely used in human activities, once they enter into water cycling system, they will be a threat to human health and ecosystem balance [6–8].

The existence of persistent organic pollutants brings challenge to wastewater treatment. Notably, the combination of adsorption and photocatalysis method is a potential strategy to better remove the pollutants in wastewater without bringing secondary pollution. Yang et al. [9,10] reported a three-dimensional hydrogel with adsorption property and high visible-light catalytic activity to remove sulfonamide antibiotics in water. Zn-Fe mixed metal oxides were developed by Di et al. and co-workers [11] to adsorb and photodegrade several pharmaceuticals and arsenic, the Zn-Fe mixed metal oxides with bifunction could efficiently remove contaminants in water. As a novel emerged class of porous materials, metal-organic frameworks (MOFs) with a number of potential applications have become a focus in the area of materials science because of the high specific surface area, controllable porous structure and well-organized framework [12,13]. It is worth noting that MOFs are great choices for adsorbing and completely photodegrading the organic pollutants in aqueous environment. Similar to semiconductors, in presence of metal centers and organic linkers, MOFs can be excited by light irradiation to gain electron-hole pairs because the organic ligands in MOFs can absorb light and activate metal clusters via a ligand-to-metal charge-transfer (LMCT) [14,15]. Therefore, the MOFs photocatalysts are being actively studied.

The discovery of UiO-66 ($Zr_6O_4(OH)_4(BDC)_{12}$) with high structural stability in water was a huge step forward in MOFs [16,17]. Since then, various strategies have been used to modify the structures and properties of UiO-66, one common method is to immobilize semiconductor or conductor on MOFs substrate to form hybrid photocatalysts and gain some unique functions [18,19]. For instance, Zhou et al. [20] have reported on efficient photodegradation of Rhodamine B (RhB) by Ag_2CO_3/UiO-66 composites, the cooperative synergism between the Ag_2CO_3 and UiO-66 in the composites might contribute to the stability and enhance the photocatalytic performance of the photocatalyst. However, most of the synthetic method is both complex and not scalable [21]. A simple and scalable modification method to achieve a superb UiO-66 photocatalyst is highly needed. Recently, there are many methods to modify the structures and properties of UiO-66. Notably, doping modification is an effective method because it has impact on pore structure and light adsorption region [22–24]. The generated photocatalytic performance might be due to the metal-to-metal charge-transfer (MMCT) excitation that producing oxo-bridged bimetallic redox site [25]. Xu et al. [26] illuminated that the doping of Fe ions into UiO-66 lattice was conductive to the photocatalytic performance for the MMCT excitation between Fe and Zr species could improve the charge separation efficiency. Based on these works, we assume that cobalt (Co) should be a promising element to be doped into UiO-66 for its excellent electrochemical properties.

Herein, Co element was adopted to synthesize a novel Co-doped UiO-66 nanoparticle by a one-step solvothermal method for the first time. The Co-doped UiO-66 nanoparticle was characterized by morphology, structure, porosity, optical performance and photoelectrochemical properties. Effects of different Zr: Co molar ratios, pH values and initial TC concentrations on adsorption removal of TC molecules were investigated. Moreover, the photocatalytic activity, mechanism and recyclability of the photocatalyst were evaluated under simulative sunlight irradiation. The novel stable Co-doped MOFs photocatalytic adsorbent showed great potential in the wastewater treatment and the methodology provided a new way to synthesis metal-doped MOFs photocatalytic adsorbent with practical application.

2. Experimental

2.1. Materials

Zirconium chloride ($ZrCl_4$), 1, 4-benzenedicarboxylic acid (H_2BDC; $C_8H_6O_4$), cobaltous chloride ($CoCl_2{\cdot}6H_2O$), N'N-Dimethylformamide (DMF; $(CH_3)_2NCHO$), ethanol (C_2H_6O) and tetracycline (TC) were of analytical reagent. Deionized water was applied as solvent in the whole experiment.

2.2. Preparation of CoUiO-66 series

CoUiO-66 series with different Co: Zr mole ratios were synthesized by a one-step hydrothermal method. Typically, H_2BDC, $ZrCl_4$ and DMF with a molar ratio of 1:1:162 were mixed in a beaker. Then, various amounts of $CoCl_2{\cdot}6H_2O$ were added respectively and kept magnetic stirring at room temperature for 1 h. Subsequently, the blue solution was placed into a Teflon reactor at 120 °C for 24 h. After nature cooling, the precipitate was separated by centrifugation, washed with DMF and ethanol for several times. Finally, the CoUiO-66 series were vacuum dried overnight at 60 °C. The final products were labeled as CoUiO-X (X = 1, 2, 4 and 8, which stand for the Zr: Co mole ratio). For comparison, the UiO-66 was also prepared in the absence of $CoCl_2{\cdot}6H_2O$ according to the same methods.

2.3. Analytical methods

The powder X-ray diffraction (XRD) was tested by Bruker AXS D8 Advance diffractometer. Field emission scanning electron microscopy (FESEM, JSM-7001F) and transmission electron microscopy (TEM, JES-3010) were used to characterize the morphology of samples. X-ray photoelectron spectroscopy (XPS) (Thermo Fisher, USA) spectrum was applied to investigate the valence state and chemical composition of samples. The N_2 adsorption-desorption isotherm and Brunauer-Emmett-Teller (BET) method were used to characterize the porous nature and surface area. The zeta potential of sample was detected by a Zeta-sizer Nano-ZS (Malvern, UK). Photoluminescence (PL) spectroscopy was recorded on FLS980 Series of Fluorescence Spectrometers at room temperature. UV–vis-NIR diffuse reflectance spectra (UV–vis-NIR DRS) was examined by a Hitachi UH-4150 spectrophotometer. Electron spin resonance (ESR) signals were detected by a Bruker ER200-SRC spectrometer under simulative sunlight. Mineralization of TC was estimated by the total organic carbon (TOC) using a Shimadzu TOC-VCPH analyzer.

2.4. Adsorption experiments

The dark adsorption experiments were conducted in 250 mL beakers containing 100 mL of 20 mg L^{-1} TC solution to investigate the adsorption of TC onto CoUiO-1, CoUiO-2, CoUiO-4, CoUiO-8 and UiO-66. Notably, 20 mg of materials were added to TC solution for the adsorption process with continuously magnetic stirring for 180 min. Samples were collected after a regular time interval and the TC concentration was measured using a UV–Vis spectrophotometer (Shimadzu, Japan).

Effect of TC solution pH values on CoUiO-1 nanoparticle adsorption capacity at the pH values of 2, 4, 6, 8, 10, 12 were estimated using dilute H_2SO_4 and NaOH solution. The zeta potentials of CoUiO-1 solutions at the pH values of 2, 4, 6, 8, 10, 12 were estimated. The TC solutions with various concentrations of NaCl, Na_2SO_4 and Na_2CO_3 were chosen to investigate the effect of coexisting anions on the adsorption performance of CoUiO-1 nanoparticle. Four TC concentrations of 10, 30, 50 and 70 mg L^{-1} were chosen to investigate the adsorption

kinetics of CoUiO-1 nanoparticle. Moreover, the thermodynamic studies were performed at three temperatures of 25 °C, 35 °C and 45 °C.

2.5. Photocatalytic experiments

Photocatalytic activity of Co-doped UiO-66 series were conducted by the photodegradation of TC with simulative sunlight irradiation. After addition of 20 mg as-prepared product into TC solution (100 mL, 20 mg L^{-1}) with continuous magnetic stirring for 1 h to get adsorption-desorption equilibrium, a 300 W Xenon lamp was used as the simulative sunlight source to irradiate the suspension. At fixed time intervals, 4 mL of samples were taken and centrifuged to detect TC concentration. The TC concentration after adsorption equilibrium was applied as zero point. Furthermore, cycle experiments were performed to verify the stability and recyclability of photocatalyst. Control experiments were carried out without addition of the as-prepared product. Photodegradation intermediates of TC were detected by the liquid chromatograph tandem mass spectrometer (LC-MS, 1290/6460 Triple Quad, USA). TC solution of 20 mg L^{-1} was prepared for degradation products identification. The detailed information of LC-MS was listed in the Supporting Information.

3. Results and discussion

3.1. Characterizations

XRD analysis could provide information on the composition and crystallinity of as-prepared samples. The XRD patterns of UiO-66 and CoUiO-X (X = 1, 2, 4, 8) were showed in Fig. 1. The characteristic peaks of UiO-66 matched well with the previous report [17], which verified the successful synthesis of UiO-66. When Co doped into UiO-66, the main diffraction peaks behaved similarly as that of UiO-66 and no diffraction peaks of Co species were found, suggesting that the doped Co was low loading and high dispersion. In addition, the Co-doped modification did not cause the phase transition of UiO-66 crystal. The doped Co element was probably incorporated into the lattice of UiO-66 [27].

The SEM images (Fig. 2a) showed that the UiO-66 sample had typical diameters of 230 nm and presented an agglomerated cubic morphology. Obviously, the CoUiO-1 sample displayed the different morphology, with dispersive and uniform cubic shape (Fig. 2b and c). The diameter of the cubes was in the range of 170 ± 10 nm. The Co-doped modification of UiO-66 caused a smaller particle size and better dispersion. Moreover, from the SEM image of CoUiO-1 nanoparticle after

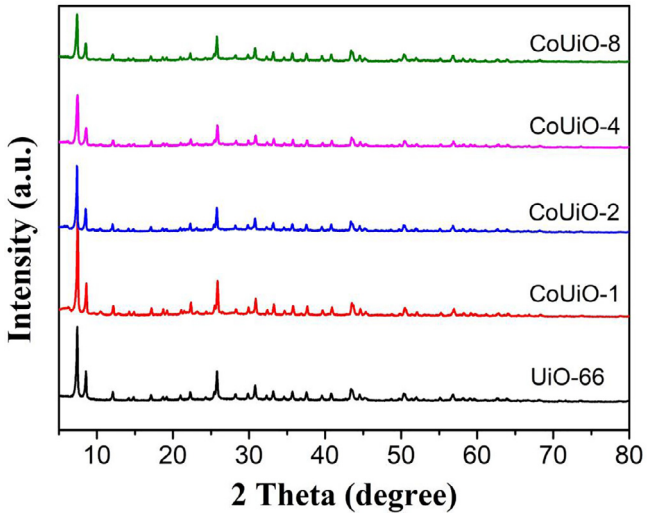

Fig. 1. XRD patterns of UiO-66 and CoUiO-X samples.

adsorptive and photocatalytic process, the CoUiO-1 nanoparticle was stable and kept the structure unchanged. No obvious particle was found in the TEM image of CoUiO-1 sample (Fig. 2e), suggesting that there was no metal or metal oxide attached on CoUiO-1 surface, which confirmed the XRD results. The EDS spectrum of the CoUiO-1 sample was obtained using the TEM (Fig. 2f). The signals of Zr, C and O in the EDS spectrum were very strong, while the signal of Co was very weak, indicating the content of Co element in CoUiO-1 sample was very low.

XPS measurement was carried out to characterize the valence state and chemical composition of CoUiO-1 sample. From the survey spectrum in Fig. 3a, the elements C, O and Zr existed in the CoUiO-1 XPS spectrum while the peak of Co was not appeared for the low content. From the ICP-AES analysis, the doped amount of Co into UiO-66 was only 0.48 wt%, which certified the XPS and EDS results of low Co content. Fig. 3b displayed the C 1s spectra of CoUiO-1, the fitting peaks at 284.0, 284.5, 285.8 and 288.7 eV were corresponded to the C—C, C═C, C—O and C═O bonds, which were attributed to the H_2BDC structure in CoUiO-1 [26]. The O 1s spectrum (Fig. 3c) could be decomposed into three peaks, which were related to Zr-O and Co-O bond (530.6 eV), C═O bond (531.5 eV) and O—H bond (532.6 eV) [28]. As shown in Fig. 3d, the binding energy peaks of Zr $3d_{5/2}$ (182.5 and 183.1 eV) and Zr $3d_{3/2}$ (184.8 and 185.5 eV) could be observed, indicating the presence of Zr^{4+} for zirconium-oxo cluster [29]. Although, the Zr: Co mole ratio was equal during the synthesis, a lot of cobalt species were washed away [30]. There were two weak peaks of Co $2p_{3/2}$ and Co $2p_{1/2}$ around 782.4 and 796.6 eV appear in the Co 2p spectrum (Fig. 3e), asserted that the doped Co was in contact with O and formed the Co-O bonds in CoUiO-1 [31]. The Co 2p spectrum indicated the dominate Co^{3+} charge state and the presence of Co^{2+} [32]. Besides, the diffraction peaks of the cobalt or cobaltic oxide species could not be observed, which proved the inexistence of cobalt or cobaltic oxide species. Therefore, the Co element was successfully doped into UiO-66.

To further investigate the surface morphology and pore volume of the as-obtained samples, the N_2 adsorption-desorption isotherms experiments were conducted and the corresponding calculated parameters of UiO-66 and CoUiO-X series were showed in Fig. 4 and Table 1. The as-obtained samples were of typical type I curve for the microporous adsorption. Compared to UiO-66, the Co-doped UiO-66 series samples attained an increased BET surface area and total pore volume (V_t). The pore size in a range from 1.35 to 1.36 nm showed ignorable change after the Co-doped modification. However, the BET surface area and V_t decreased with the increase of Co content, indicating that Co doped into the pore successfully and it has impact on pore structure and surface area of UiO-66. Nevertheless, large BET surface area and pore volume of CoUiO-X series could offer more active sites which were favorable for improving the adsorption capacity and photocatalytic activity.

3.2. Adsorption removal of TC

3.2.1. Different CoUiO-X samples

As shown in Fig. 5, the equilibrium adsorption for TC molecules was investigated. All curves showed a rapid adsorption between t = 0 and 10 min, and a very slow adsorption at longer time. A poor adsorption capacity (11.2 mg g^{-1}) could be obtained on UiO-66 while the CoUiO-X series exhibited an improved adsorption capacity. As the increase in Co content, the TC adsorption capacity of CoUiO-X series showed an upward trend. Notably, the CoUiO-1 nanoparticle exhibited a maximum adsorption capacity of 85.1 mg g^{-1}. The enhanced adsorption capacity may be due to that the doped Co element in UiO-66 donated valence electron, which was beneficial for TC molecules to be bind to the metal centers [33].

3.2.2. Effect of adsorbent dosage and coexisting anions

For the adsorption studies, the optimization of adsorbent dosage was necessary. In Fig. 6a, the increasing the dosage of CoUiO-1

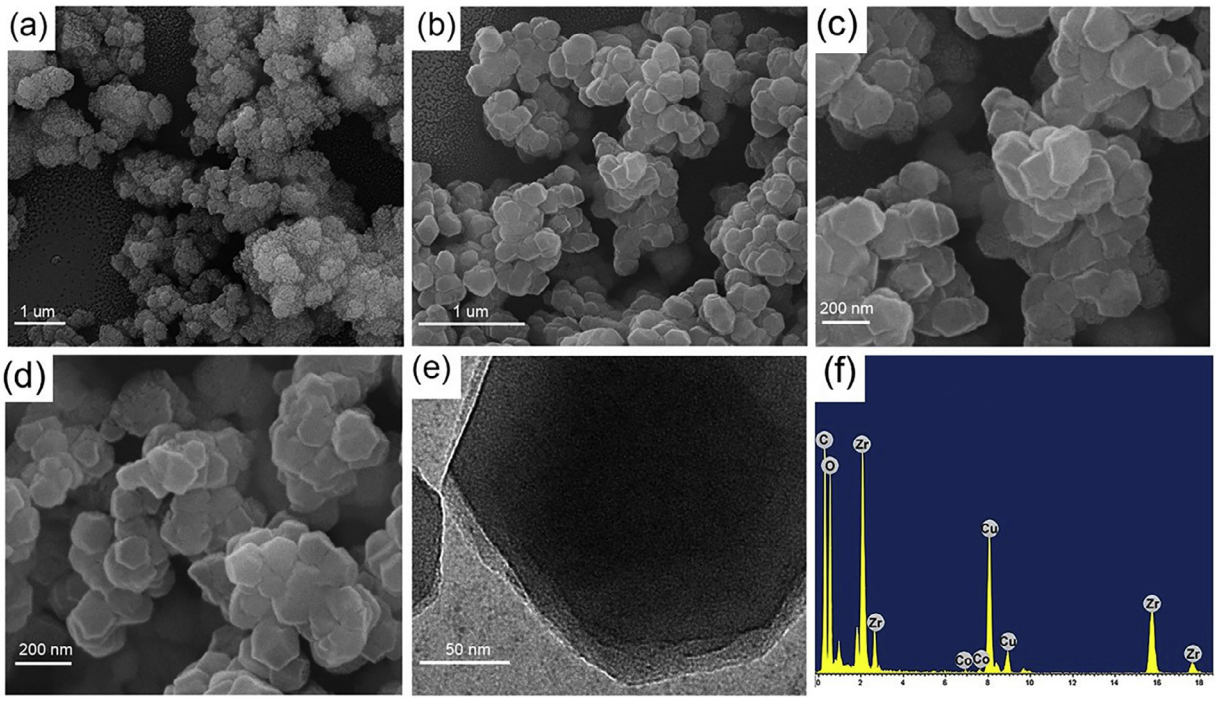

Fig. 2. SEM images of UiO-66 (a) and CoUiO-1 (b and c) with different magnification; SEM image of CoUiO-1 after adsorptive and photocatalytic process (d); TEM images (e) and EDS spectrum (f) of CoUiO-1.

nanoparticle range from 0.2 to 1.2 g L^{-1} did enhance the removal efficiency of TC for the higher adsorbent concentration could translate into more adsorption sites [34]. However, there was a negative correlation between the adsorbent dosage and adsorption capacity due to the interaction of active sites of adsorbents [35]. Notably, high TC removal efficiencies (> 90%) were achieved at a dosage of 0.4 to 1.2 g L^{-1}.

Generally, there were other ions like Cl^-, SO_4^{2-} and CO_3^{2-} coexisted in actual wastewater with TC molecules. Fig. 6b showed the influence of various concentrations of Cl^-, SO_4^{2-} and CO_3^{2-} on TC removal by CoUiO-1 nanoparticle. As the Fig. 6b showed, with the addition of Cl^-, SO_4^{2-} and CO_3^{2-}, the adsorption ability of TC decreased as the ions concentrations increased. Moreover, the influence of coexisting ions followed the order: $SO_4^{2-} > CO_3^{2-} > Cl^-$. The adding anions could complete the active sites with TC molecules and the result proved that the anions with more negative charge caused stronger bond with the adsorbent [36].

3.2.3. Effect of solution pH

The pH value of the TC solution had a strong impact on the adsorption performance of CoUiO-1 nanoparticle and the existing state of TC molecules. As shown in Fig. 7, a series of pH values of TC solution were applied to investigate the effect of initial pH values on TC adsorption. The adsorption capacity of 17.2 mg g^{-1} at pH 2 was increased to 108.4 mg g^{-1} as the pH of 10. The adsorption capacity then dramatically decreased at pH 12. Notably, the maximum adsorption capacity was displayed at pH 10. The trend of TC adsorption was further predicted by zeta potential measurements of the CoUiO-1 dispersions in TC solution. Table S1 summarized the surface charge of the CoUiO-1 nanoparticle and TC molecules at various pH values and the dominant interaction in adsorption process.

TC molecules were sensitive to pH values on account of their protonation state[37]. The surface charge of CoUiO-1 nanoparticle was positive below pH 10 while negative beyond pH 10. Meanwhile, the TC molecules could form three species in aqueous solutions under different pH values, including cationic species (pH < 3.3), zwitter ionic species (3.3 < pH < 7.7) or anionic species (pH > 7.7). In this case, the TC adsorption on CoUiO-1 nanoparticle was obviously affected by pH values, so that the electrostatic interaction was dominate interaction in the adsorption process. The poor TC adsorption capacity of CoUiO-1 nanoparticle at pH 2 was due to the electrostatic repulsion hindering the adsorption performance for the surface charge of TC molecules and CoUiO-1 nanoparticle were like charged. At pH 4, the surface charge of TC molecules was neutral while CoUiO-1 nanoparticle was positive, the electrostatic attraction promoted the adsorption process. In the pH range of 6–10, the surface charge of TC changed from neutral to negative while the surface charge of CoUiO-1 nanoparticle was positive. However, adsorption capacity was still high, suggesting the π-π interaction between the organic linker and the aromatic structure in TC molecules was dominant at the pH values between 4 and 10 [38]. The decreased adsorption capacity at pH 12 was due to the electrostatic repulsion [39]. Obviously, the point of zero charge was obtained at pH 10.

3.2.4. Effect of initial TC concentrations

Adsorption of TC with different initial concentrations on CoUiO-1 nanoparticle was performed at pH 10. As showed in Fig. 8, the TC concentration had great impact on the adsorption process, where 99.8%, 91%, 71.3% and 60.3% of TC were removed at TC concentration of 10, 30, 50 and 70 mg L^{-1}, respectively. The initial TC concentrations ranging from 10 to 70 mg L^{-1}, the adsorption capacity increased with an increasing TC concentration of solution (the adsorption capacity could reach up to 224.1 mg g^{-1} at TC concentration of 70 mg L^{-1}), which could be due to that a higher initial TC concentration would result in higher driving force of the concentration gradient [40]. The adsorption equilibrium could be attained at 60 min, especially at TC concentration of 10 mg L^{-1}, almost all the TC molecules were adsorbed within 10 min. In the first few minutes, there were abundant adsorption sites for TC molecules, which could be a reason of the high initial uptake amount. Later, the forces of repulsion between the TC molecules in solution and the adsorbed TC molecules on CoUiO-1 nanoparticle surface leaded to the low adsorption capacity.

To further investigate the adsorption process, adsorption kinetics experiments of TC on CoUiO-1 were conducted at TC concentration of 10, 30, 50 and 70 mg L^{-1}. As presented in Fig. S1 and Table S2, the

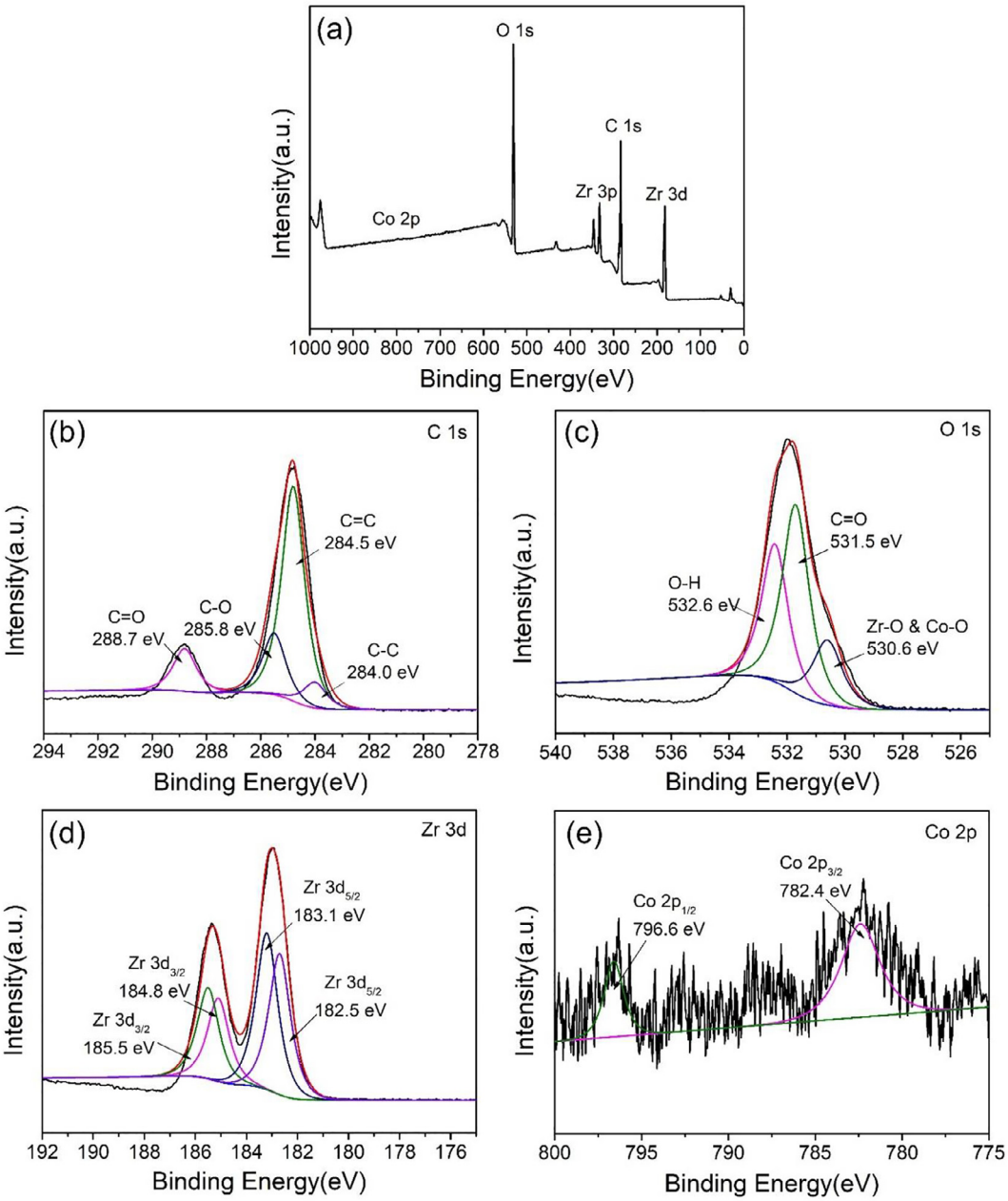

Fig. 3. XPS spectra of CoUiO-1 sample: (a) survey, (b) C 1s, (c) O 1s, (d) Zr 3d and (e) Co 2p.

pseudo-second-model showed fitting better than pseudo-first-order model for the higher correlation coefficients ($R^2 > 0.999$). Moreover, better approximation could be obtained between the calculated adsorption capacity ($q_{e,cal}$) and the experimental adsorption capacity ($q_{e,exp}$) by the pseudo-second-order model. Therefore, the chemisorption was relatively dominant in the adsorption process [41]. The intraparticle diffusion model was applied to investigate the diffusion of TC molecules into the pores of CoUiO-1. As shown in Fig. S1 and Table S2, all the plots displayed two linear sections. In the first stage, the curves with large slope indicated a rapid TC adsorption process due to the existence of abundant active sites on the surface of CoUiO-1 nanoparticle. With the increase of TC concentration, a higher driving force of the concentration gradient was reached for rapid TC molecules diffusion and adsorption on the active sites of CoUiO-1 surface. In the second stage, the curves with small slope suggested the adsorption rate decreased as the intraparticle diffusion process for the active sites were fully occupied. In this stage, the adsorption process slowly reached to adsorption equilibrium. Furthermore, the C_i value of each curve was not zero, indicating that intraparticle diffusion was not governed by the sole rate-limiting step and TC adsorption by CoUiO-1 nanoparticle included both intra-particle diffusion and outer diffusion process [42].

3.2.5. Adsorption isotherm and thermodynamic studies

The reaction behavior between the equilibrium solution concentration C_e (mg L^{-1}) and the adsorption capacity q_e (mg g^{-1}) at constant temperature could be analyzed by adsorption isotherm. The experimental data was described by three isotherm models (Langmuir, Freundlich and Temkin models). As showed in Fig. S2 and Table S3, the adsorption of TC on CoUiO-1 nanoparticle showed a good fit with Freundlich model, indicating that it ought to be multilayer adsorption on a heterogeneous surface at room temperature[43]. In general, it was hard to adsorb when $1/n > 2$, while $0.1 < 1/n < 0.5$ meant the adsorption was easy to be performed[44]. In this case, the 1/n (0.217) value was much less than 0.5, which implied an excellent adsorption

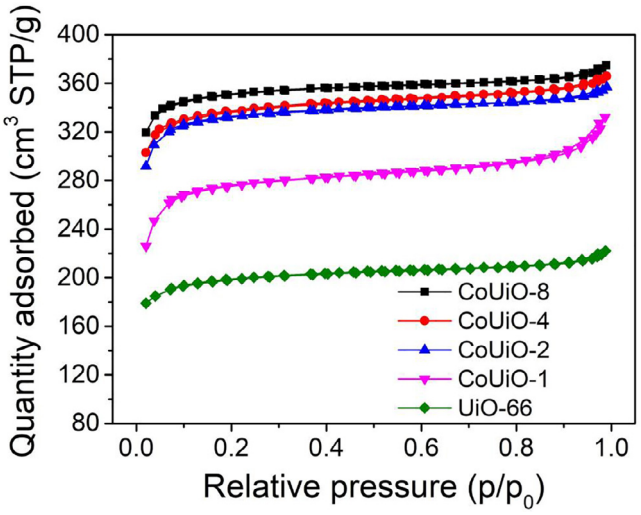

Fig. 4. The N_2 adsorption-desorption isotherms of UiO-66 and CoUiO-X samples.

Table 1
Surface area, pore size and pore volume parameters for various materials.

Samples	Surface area[a] (m^2g^{-1})	Pore size[b] (nm)	V_t[c] (m^3g^{-1})
UiO-66	584.44	1.35	0.34
CoUiO-1	815.18	1.36	0.51
CoUiO-2	974.37	1.36	0.55
CoUiO-4	986.74	1.35	0.57
CoUiO-8	1024.71	1.35	0.58

[a] Measured using N2 adsorption with the Brunauer–Emmett–Teller (BET) method.

[b] Pore size in diameter calculated by the desorption data using Barrett–Joyner–Halenda (BJH) method.

[c] Total pore volume determined at P/P0 = 0.99.

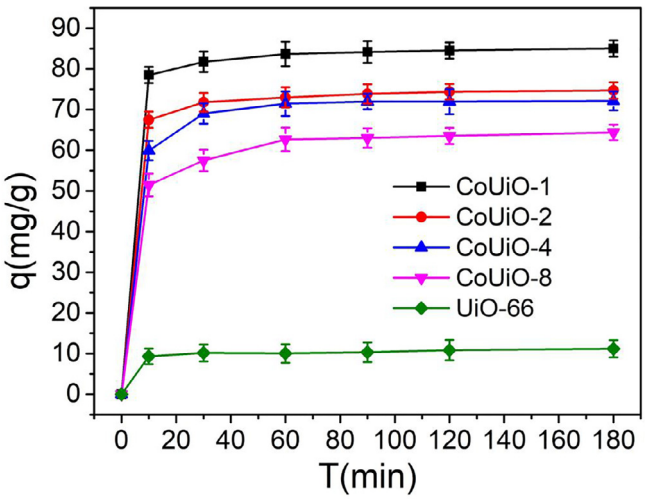

Fig. 5. TC adsorption performance of UiO-66 and CoUiO-X (Experimental conditions: initial TC concentration = 20 mg L^{-1}; pH = 5.37; m = 20 mg; V = 100 mL).

process[45]. The high R^2 (0.99426) also manifested there was a strong interaction between CoUiO-1 nanoparticle and TC molecules.

We also investigated the effect of temperature on TC adsorption by CoUiO-1 nanoparticle. As showed in Fig. 9, the adsorption capacity and removal efficiency of CoUiO-1 increased as the temperature increased. The thermodynamic analysis results were listed in Table 2. The positive ΔS and ΔH values indicated that the TC adsorption on CoUiO-1 nanoparticle was an endothermic process in which entropy was increased, while the negative ΔG value manifested the adsorption process was spontaneous [46]. Furthermore, the TC adsorption capacities of the adsorbents from previous studies were listed in Table 3. Table 3 showed that the adsorption capacity of the as-prepared CoUiO-1 nanoparticle was higher than those previously reported, suggesting that CoUiO-1 nanoparticle was a promising adsorbent for the TC removal.

3.3. Photocatalytic removal of TC

The TC photodegradation experiments of CoUiO-X series were evaluated under simulative sunlight illumination after dark adsorption process. After 1 h of adsorption process, the removal efficiencies of UiO-66, CoUiO-1, CoUiO-2, CoUiO-4 and CoUiO-8 were 9.9%, 68.1%, 61.3%, 58.6% and 55.4%, respectively (Fig. 10a). The TC concentration after adsorption equilibrium was applied as the zero point. As shown in Fig. 10b, the TC was stable without any photocatalyst under irradiation while CoUiO-X series showed higher photocatalytic activity than that of pure UiO-66. Notably, the photocatalytic performance of TC increased with increasing Co content and the CoUiO-1 nanoparticle demonstrated the highest performance. The degradation efficiency of CoUiO-1 nanoparticle was 78.5% under irradiation. The enhanced efficiency may be attributed to the better adsorption property of TC molecules, the stronger light adsorption and the higher charge separation efficiency. Moreover, TOC removal of 13.8% could be obtained after 1 h of sunlight irradiation. Fig. 10c showed UV–vis-NIR diffuses reflectance spectra (DRS) of UiO-66 and CoUiO-X series. Compared to UiO-66, the CoUiO-X series showed a stronger adsorption in UV region and an extra adsorption spectrum in visible region. Notably, the absorption band of CoUiO-X series even extended to the infrared region. The improved light adsorption was considered to enhance the photocatalytic activity of CoUiO-X series towards TC molecules. Obviously, the optical absorption edges of UiO-66 and CoUiO-X series were similar and found at 340 nm, indicating that they were UV-driven photocatalysts and had wide band gaps approximately of 3.64 eV. However, for CoUiO-X series, the absorption edge of them had no obvious red shift with increasing amount of Co. As the result of ICP-AES analysis, the amount of Co was very limited and the host crystal of the product was still UiO-66, so that the Co-doped modification did not virtually change the band gap of UiO-66 [31]. It had been reported that the metal-doped modification could cause an extra adsorption band without changing the inherent absorption edge [47]. Thus, the CoUiO-X series could respond to visible light.

The charge separation of electron-hole pairs of semiconductor was also investigated by PL spectroscopy under 319 nm at 298 K. The emission peaks at approximately 397 nm of UiO-66 and CoUiO-1 were observed. Generally, the PL signals were closely associated with the recombination of photogenerated carriers. As showed in Fig. 10d, the CoUiO-1 nanoparticle presented a lower PL intensity compared to UiO-66, which meant the Co-doped modification leaded to lower recombination rate of electron-hole pairs and higher photocatalytic performance. To further investigate the effect of Co-doped modification on the separation efficiency of photoinduced carriers, the electrochemical measurements were performed under simulative sunlight irradiation. Fig. 10e and f showed the results of photoelectric current and electrochemical impedance spectroscopy (EIS) experiments. The transient photocurrent of CoUiO-1 was about 3 times than that of pure UiO-66, the enhancement of transient photocurrent of CoUiO-1 sample indicated the photoinduced carriers were separated effectively and the photoinduced carriers had a longer lifetime [18]. The same result was obtained from EIS experiment. Fig. 10f showed the EIS changes of UiO-66 and CoUiO-1 samples. The UiO-66 sample showed a bigger diameter, which proved that the poor electrical conductivity of UiO-66 may hinder the transfer of photoinduced carriers. Notably, the CoUiO-1 sample showed smaller arc radius than that of UiO-66, which could be attributed to the Co-doped modification. In most case, a smaller arc

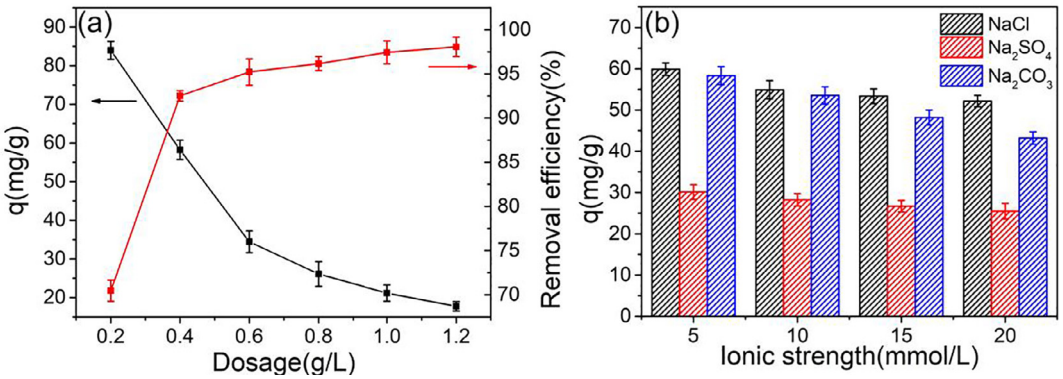

Fig. 6. (a) Effect of adsorbent dose on TC adsorption by CoUiO-1 nanoparticle (Experimental conditions: initial TC concentration = 20 mg L^{-1}; pH = 5.37; m = 20–120 mg; V = 100 mL); (b) effect of coexisting anions (Cl^-, SO_4^{2-}, and CO_3^{2-}) on TC adsorption by CoUiO-1 nanoparticle (Experimental conditions: initial TC concentration = 20 mg L^{-1}; pH = 5.37; m = 20 mg; V = 100 mL).

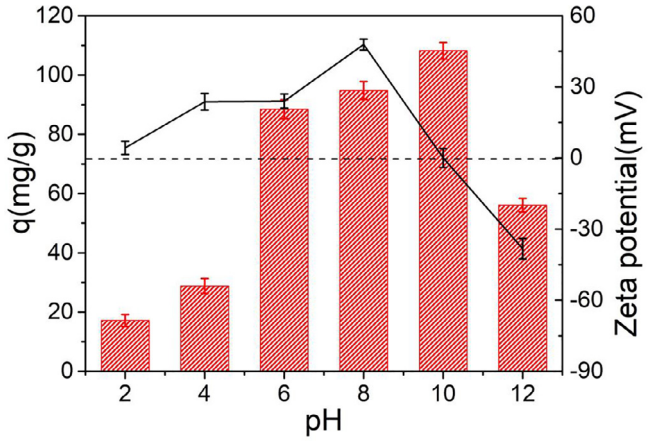

Fig. 7. Effect of pH values on TC adsorption by CoUiO-1 (a); zeta potentials (b) of CoUiO-1 (Experimental condition: initial TC concentration = 20 mg L^{-1}; m = 20 mg; V = 100 mL).

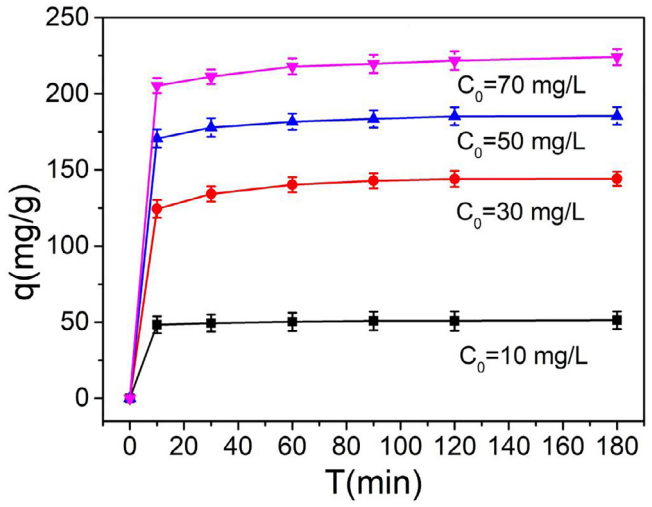

Fig. 8. Effect of different initial TC concentrations (Experimental conditions: m = 20 mg; V = 100 mL, pH = 10) on the adsorption of TC onto CoUiO-1.

radius meant a smaller charge-transfer resistance. Therefore, the CoUiO-1 sample had the highest efficiency in charge separation. These results were in accordance with the PL analysis, which confirmed that the Co-doped modification was contributed to photocatalytic performance.

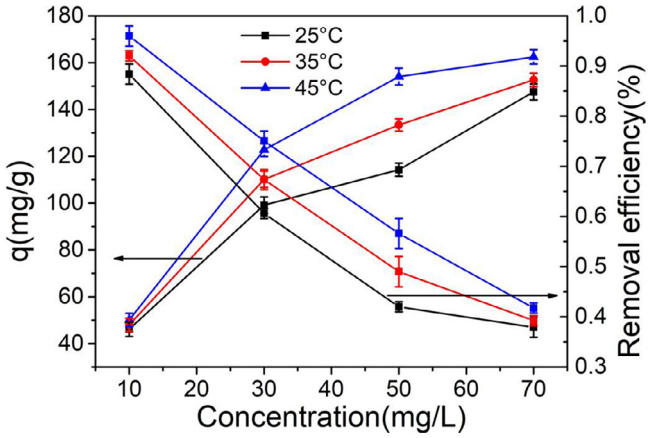

Fig. 9. Effect of different temperature (Experimental conditions: m = 20 mg; V = 100 mL, pH = 5.37) on the adsorption of TC onto CoUiO-1.

Table 2
Thermodynamic parameters for adsorption of TC on the CoUiO-1 nanoparticle.

Pollutants	T (K)	ΔG (kJ mol^{-1})	ΔH (kJ mol^{-1})	ΔS (kJ mol^{-1} K^{-1})
TC	298	−1.671	41.539	0.145
	308	−3.121		
	318	−4.571		

Table 3
Comparison of the CoUiO-1 adsorbent with other materials on TC adsorption at room temperature.

Adsorbent	q_{max} (mg g^{-1})	Reference
Fe_3O_4@SiO_2-Chitosan/GO	151.4	[56]
NH_2-MIL-101(Cr)	14	[57]
Zn-AC	51.65	[58]
Cu_2O-TiO_2-Pal	113.6	[59]
In_2S_3@MIL-125(Ti)	154.3	[37]
$GBCM_{350}$ activated carbon	58.2	[60]
MIL-101(HCl)	39.88	[61]
UiO-66	23.1	[62]
ZIF-8	140.54	[63]
CoUiO-1	224.1	This work

3.3.1. Photocatalytic mechanism

The active species trapping experiments were conducted to investigated the photodegradation mechanism of CoUiO-1 nanoparticle (Fig. 11a). Three radical scavengers, ammonium oxalate (AO), isopropyl alcohol (IPA) and p-benzoquinone (BQ), were used to capture

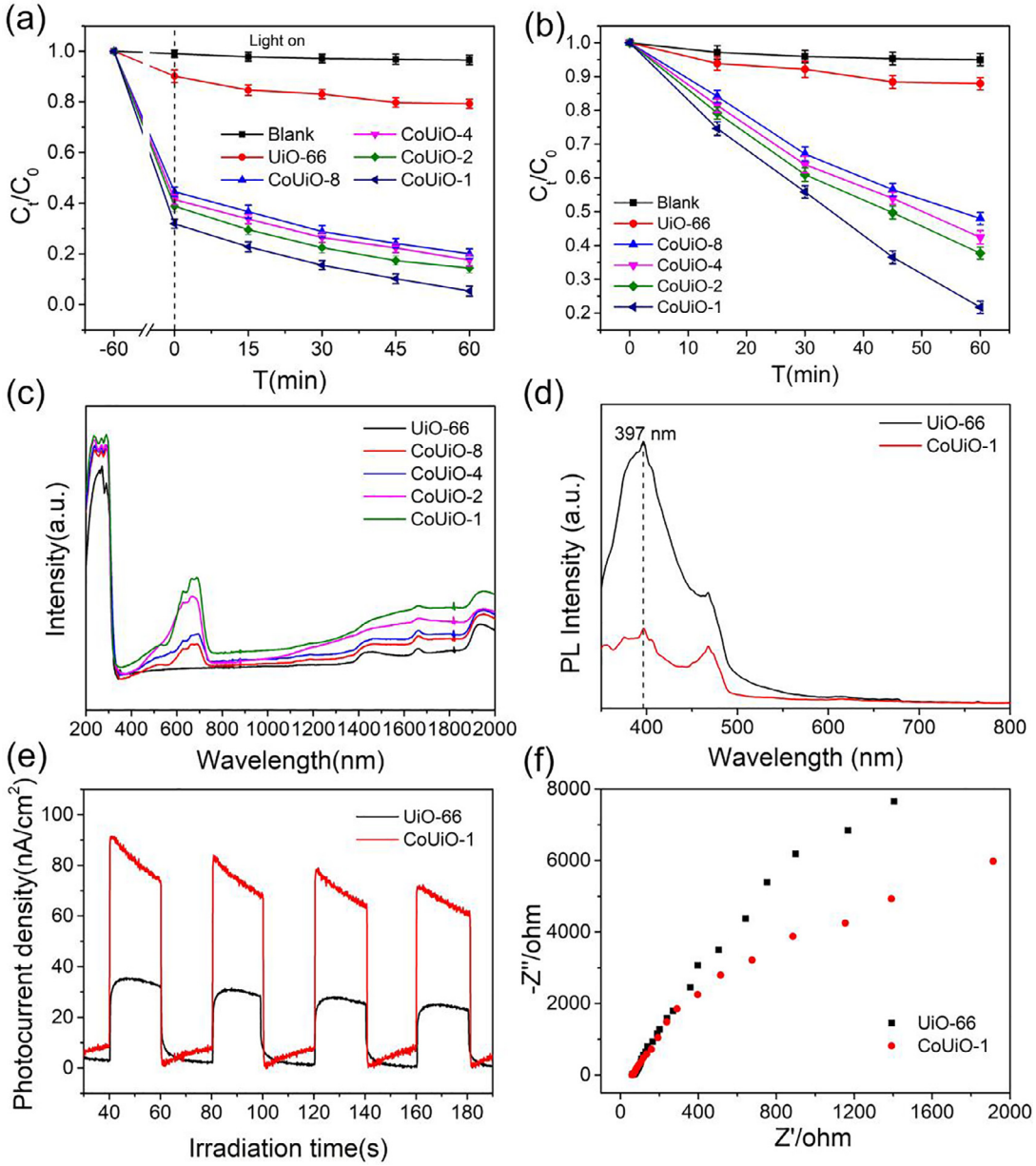

Fig. 10. TC degradation performance of photocatalysts under simulative sunlight irradiation (a and b) (Experimental conditions: initial TC concentration = 20 mg L^{-1}; pH = 5.37; m = 20 mg; V = 100 mL); UV–vis-NIR DRS spectra of as-obtained samples (c); PL emission spectra of UiO-66 and CoUiO-1 (d); transient photocurrent responses (e) and EIS changes of UiO-66 and CoUiO-1 sample.

hole (h^+), superoxide radical ($\cdot O_2^-$) and hydroxyl radical (·OH) [48], respectively. From Fig. 11b, after the addition of IPA and BQ, the degradation efficiency of TC was significantly suppressed, especially after adding BQ, the degradation efficiency was only 15.6%. Therefore, the $\cdot O_2^-$ and ·OH species were the main active species that could efficiently facilitate the TC degradation. The ESR measurements were employed to verify the results of trapping experiments. Fig. 11c and d showed the ESR signals of DMPO-$\cdot O_2^-$ and DMPO-·OH. No signals were found in the dark, while the characteristic peaks of DMPO-$\cdot O_2^-$ and DMPO-·OH adducts were observed after 5 min of irradiation. These results demonstrated that the CoUiO-1 could be excited by light irradiation to generate $\cdot O_2^-$ and ·OH species.

According to the previous literature [30,49], we proposed the possible photocatalytic mechanism in Fig. 12. The TC molecules could be adsorbed by the benzene structure in CoUiO-1 nanoparticle, which was beneficial to the photocatalytic process. Under simulative sunlight irradiation, the organic ligands H_2BDC were excited, then the excited ligands transferred photoelectrons to the Zr-O cluster to form Zr^{3+} (LMCT). The as-formed Zr^{3+} could react with O_2 to generate $\cdot O_2^-$ while Zr^{3+} was oxidized back to Zr^{4+} [37,50]. The Co element served as a mediator, so that the photogenerated electrons could be immediately captured, which greatly improved the transfer of photoelectrons and minimized recombination of photoinduced carriers [51]. Though the doped Co amount was negligible, it played a vital role in electron transfer. The oxidizing Co^{3+} could be reduced to Co^{2+} by photoelectron, meanwhile, the unstable Co^{2+} was readily regenerated to Co^{3+}. Then the photogenerated electrons could reacted with O_2 to generate $\cdot O_2^-$ and subsequently yielded ·OH. The oxidizing $\cdot O_2^-$ and ·OH radicals could effectively degraded TC molecules into other products. Moreover, the synergistic effect of Co and Zr species was conducive to enhance charge separation, which was based on MMCT excitation [52]. The higher separation and transfer of photogenerated carriers of CoUiO-1 nanoparticle was proved by the photoelectric current and electrochemical impedance spectroscopy results mentioned above.

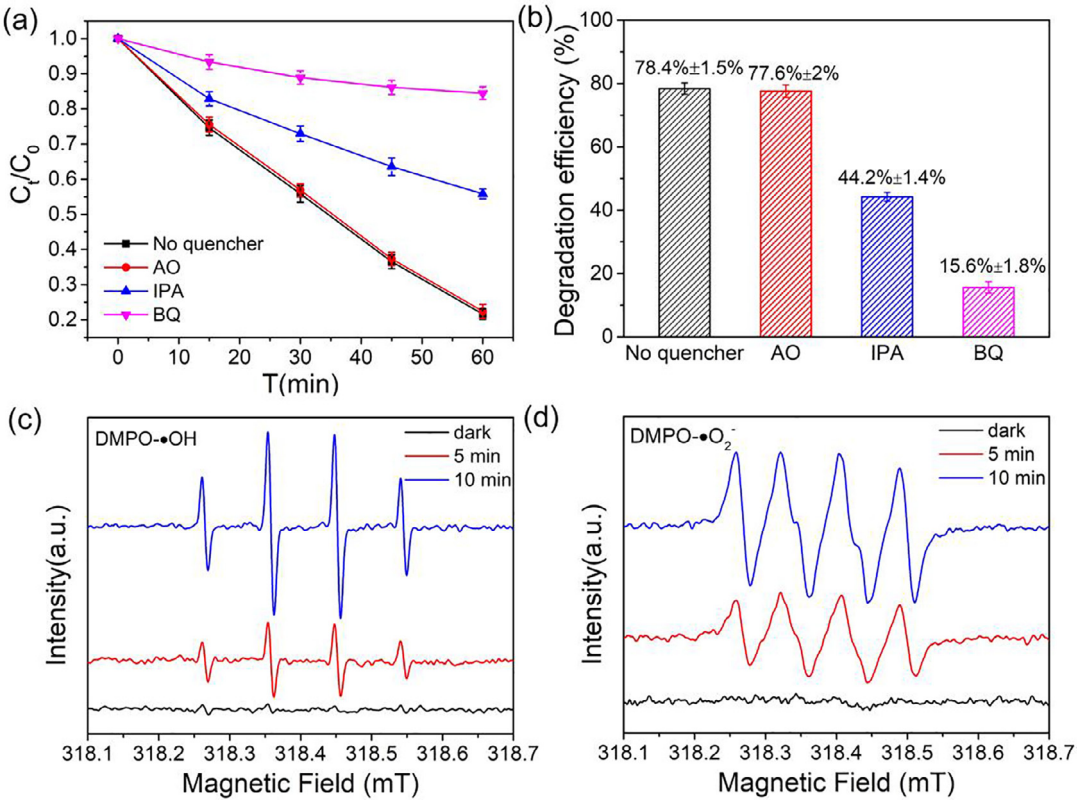

Fig. 11. Effects of different radical scavengers on photodegradation of TC by CoUiO-1 under simulative sunlight irradiation (a and b); DMPO spin-tripping ESR spectra for CoUiO-1 in aqueous dispersion for DMPO-·O_2^- (c) and methanol dispersion for DMPO-·OH (d).

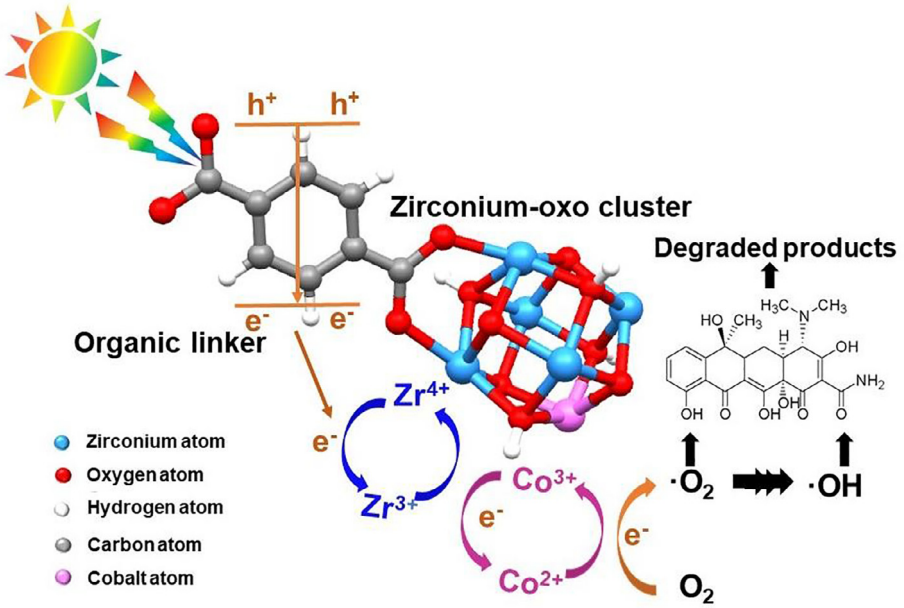

Fig. 12. The proposed photocatalytic mechanism for the TC degradation on CoUiO-1 under simulative sunlight irradiation.

3.3.2. *TC photodegradation pathway*

The TC intermediates were detected by LC-MS during the photocatalytic process to investigate its degradation pathway and mechanism. The product with m/z = 455 was corresponded to the molecular weight of TC. After simulative sunlight irradiation for 60 min, ten intermediates were identified by LC-MS and the probable TC degradation pathway was proposed. Possible two main pathways were presented in Fig. 13. The pathway I was mainly the addition reaction of carbon–carbon double bond. The carbon–carbon double bond in TC was attacked by ·OH to generate product 1 with m/z = 461.2. Subsequently, the product 1 was continuously attacked by ·OH and changed to product 2 (m/z = 477.3). This product then transformed to the product 3 (m/z = 449.4) by the dealkylation [53]. The product 3 could be further attacked by ·OH to break the carboatomic ring and generated product 4 (m/z = 363.1). The pathway II was mainly included dealkylation and dehydration process. The dehydration of TC could form product 5 ($m/$

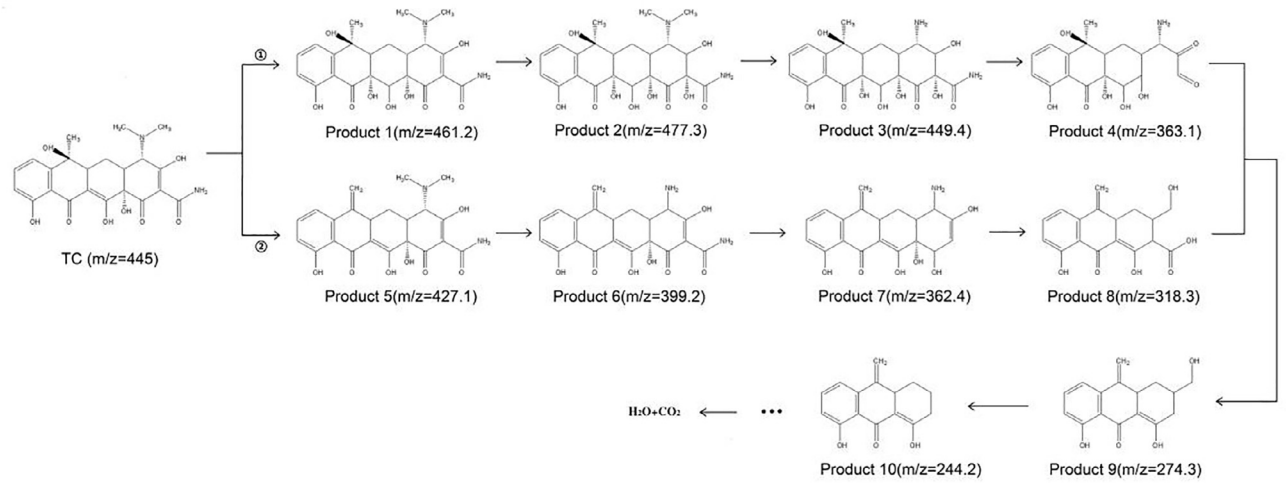

Fig. 13. The proposed transformation pathways of TC degradation.

z = 427.1) and then lost the N-methyl group to generate product 6 (m/z = 399.2). After further attacked by active radicals, the acylamino of product 6 could be removed and generated product 7 (m/z = 362.4). Because of the strong oxidizing ·OH and $\cdot O_2^-$, the carboatomic ring in product 6 could be cleavage to generate product 8 (m/z = 318.3). This pathway was similar to the previous researches [54]. The product 4 and product 8 could be further oxidized by ·OH and $\cdot O_2^-$ to gain an intermediate with m/z = 274.3 (product 9). Then, the product 10 with m/z = 244.2 was found by losing the methanol in carboatomic ring. Ultimately, the above ring-opening products (product 4, product 8, product 9 and product 10) were oxidized into CO2 and H2O.

3.3.3. Photocatalyst recyclability

The CoUiO-1 nanoparticle was gathered and ultrasonic washed after the photocatalytic process and dried in 60 °C vacuum to perform the recycle experiments under the same conditions. As shown in Fig. 14a, after four runs, the CoUiO-1 nanoparticle had a little loss of photocatalytic activity. Moreover, Fig. 14b showed the XRD patterns of CoUiO-1 nanoparticle of fresh and after reused for four runs. After four runs, no obvious change was observed, indicating the CoUiO-1 nanoparticle was stable and recyclable in terms of photodegradation of TC.

3.3.4. Preliminary experiment of CoUiO-1 on real samples

Considering the complex composition of the real wastewater, we investigated the application of CoUiO-1 nanoparticle in the treatment of real samples. Ultrapure water, tap water, river water and pharmaceutical wastewater samples were applied as the solution to prepare the TC solution of 20 mg L^{-1} (the dosage of CoUiO-1 was 0.2 g L^{-1}). After the adsorption and photocatalytic process, the TC removal efficiencies of ultrapure water, tap water, river water and pharmaceutical wastewater were 94.6%, 91.7%, 88.5% and 87.1%, respectively. The quality parameters of tap water, river water and pharmaceutical water were listed in Table 4. It could be concluded that the competitive anions and organic matters had effect on the adsorption performance and photocatalytic activity [55]. Therefore, the CoUiO-1 photocatalytic adsorbent showed large adsorption capacity and high photocatalytic efficiency, which was potential in wastewater treatment.

4. Conclusion

In this work, we synthesized a novel recyclable Co-doped UiO-66 photocatalytic adsorbent by a one-step solvothermal method. The doped Co element greatly enhanced adsorption capacity and photocatalytic activity of UiO-66. Notably, the CoUiO-66 with Zr: Co molar ratio of 1:1 (CoUiO-1) displayed the highest adsorption capacity and photocatalytic performance. The CoUiO-1 nanoparticle showed a high adsorption capacity of 224.1 mg g^{-1}, then the adsorbed TC molecules could be degraded more than 94% of initial concentration under simulative sunlight irradiation. The high adsorption capacity was due to the π-π interaction and electrostatic interaction between CoUiO-1 nanoparticle and TC molecules. We also found that the adsorption process was strongly depended on adsorbent dosage, coexisting ions, pH values and initial TC concentrations. The thermodynamic study indicated the TC adsorption on CoUiO-1 nanoparticle was a spontaneous and

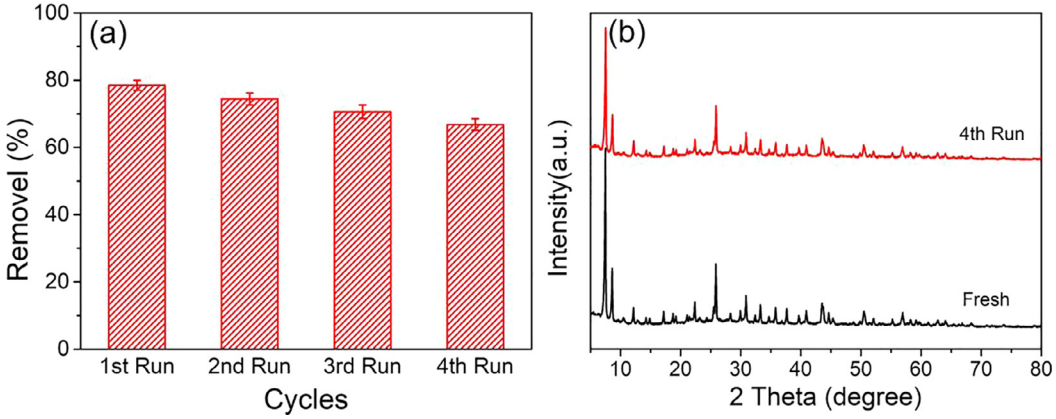

Fig. 14. Recycling tests of the photodegradation of TC over CoUiO-1 photocatalytic adsorbent under sunlight irradiation(a); XRD patterns of CoUiO-1 before and after photocatalytic process.

Table 4
The quality parameters of tap water, river water and pharmaceutical wastewater.

Parameters	Tap water	River water[a]	Pharmaceutical wastewater[b]
pH	7.51	7.75	6.78
COD	2.139 mg L^{-1}	42.25 mg L^{-1}	24100 mg L^{-1}
TOC	0.723 mg L^{-1}	16.75 mg L^{-1}	5021.16 mg L^{-1}
Main contents	Chloride, sulfate, nitrate	Chloride, sulfate, bromide	Bufexamac, methanol, ethanol, hydroxylamine, 1-bromobutane

[a] The river water was obtained from Xiang river in Hunan province.
[b] The pharmaceutical wastewater sample was diluted 100 times when applied in the adsorptive and photocatalytic experiments.

exothermic process. Furthermore, the TC photodegradation of CoUiO-1 nanoparticle under simulative sunlight displayed the Co-doped modification caused an extra light absorption and facilitated the electron transfer, which was beneficial to enhance the photocatalytic performance. A plausible degradation pathway for TC was proposed and part of TC may be mineralized to CO_2 and H_2O. Moreover, the CoUiO-1 nanoparticle was effective to the treatment of real samples including tap water, river water and pharmaceutical wastewater. These results provided a new way to synthesis a stable transition metal-doped MOFs photocatalytic adsorbent for efficiently removal of contaminants like TC in wastewater.

Acknowledgements

The study was financially supported by the National Natural Science Foundation of China (51578223 and 51521006) and the Key Research and Development Program of Hunan Province (2017SK2242).

Appendix A. Supplementary data

Supplementary data associated with this article can be found, in the online version, at https://doi.org/10.1016/j.cej.2018.07.060.

References

[1] L. Tang, G.M. Zeng, G.L. Shen, Y.P. Li, Y. Zhang, D.L. Huang, Rapid Detection of Picloram in Agricultural Field Samples Using a Disposable Immunomembrane-Based Electrochemical Sensor, Environ. Sci. Technol. 42 (2008) 1207.
[2] Z.H. Yang, R. Xu, Y. Zheng, T. Chen, L.J. Zhao, M. Li, Characterization of extracellular polymeric substances and microbial diversity in anaerobic co-digestion reactor treated sewage sludge with fat, oil, grease, Bioresour. Technol. 212 (2016) 164.
[3] Z. Cetecioglu, B. Ince, M. Gros, S. Rodriguez-Mozaz, D. Barceló, Chronic impact of tetracycline on the biodegradation of an organic substrate mixture under anaerobic conditions, Water Res. 47 (2013) 2959–2969.
[4] C. Zhou, C. Lai, D. Huang, G. Zeng, C. Zhang, M. Cheng, L. Hu, J. Wan, W. Xiong, M. Wen, Highly porous carbon nitride by supramolecular preassembly of monomers for photocatalytic removal of sulfamethazine under visible light driven, Appl. Catal. B 220 (2017).
[5] P. Song, Z. Yang, G. Zeng, X. Yang, H. Xu, L. Wang, R. Xu, W. Xiong, K. Ahmad, Electrocoagulation treatment of arsenic in wastewaters: a comprehensive review, Chem. Eng. J. (2017).
[6] R. Xu, Z.H. Yang, Q.P. Wang, Y. Bai, J.B. Liu, Y. Zheng, Y.R. Zhang, W.P. Xiong, K. Ahmad, C.Z. Fan, Rapid startup of thermophilic anaerobic digester to remove tetracycline and sulfonamides resistance genes from sewage sludge, Sci. Total Environ. 612 (2017) 788.
[7] Y. Zhou, X. Liu, Y. Xiang, P. Wang, J. Zhang, F. Zhang, J. Wei, L. Luo, M. Lei, L. Tang, Modification of biochar derived from sawdust and its application in removal of tetracycline and copper from aqueous solution: Adsorption mechanism and modelling, Bioresour. Technol. 245 (2017) 266.
[8] C. Zhou, C. Lai, P. Xu, G. Zeng, D. Huang, C. Zhang, M. Cheng, L. Hu, J. Wan, Y. Liu, In situ grown AgI/$Bi_{12}O_{17}Cl_2$ heterojunction photocatalysts for visible light degradation of sulfamethazine: efficiency, pathway and mechanism, ACS Sustainable Chem. Eng. (2018).
[9] H. Yi, G. Zeng, C. Lai, D. Huang, L. Tang, J. Gong, M. Chen, P. Xu, H. Wang, M. Cheng, Environment-friendly fullerene separation methods, Chem. Eng. J. 330 (2017).
[10] J. Yang, Z. Li, H. Zhu, Adsorption and photocatalytic degradation of sulfamethoxazole by a novel composite hydrogel with visible light irradiation, Appl. Catal. B 217 (2017) 603–614.
[11] G. Di, Z. Zhu, H. Zhang, J. Zhu, H. Lu, W. Zhang, Y. Qiu, L. Zhu, S. Küppers, Simultaneous removal of several pharmaceuticals and arsenic on Zn-Fe mixed metal oxides: Combination of photocatalysis and adsorption, Chem. Eng. J. 328 (2017) 141–151.
[12] H.B. Wu, B.Y. Xia, L. Yu, X.Y. Yu, X.W. Lou, Porous molybdenum carbide nano-octahedrons synthesized via confined carburization in metal-organic frameworks for efficient hydrogen production, Nat. Commun. 6 (2011).
[13] W.P. Xiong, G.M. Zeng, Z.H. Yang, Y.Y. Zhou, C. Zhang, M. Cheng, Y. Liu, L. Hu, J. Wan, C.Y. Zhou, R. Xu, X. Li, Adsorption of tetracycline antibiotics from aqueous solutions on nanocomposite multi-walled carbon nanotube functionalized MIL-53 (Fe) as new adsorbent, Sci. Total Environ. 627 (2018) 235–244.
[14] T. Tachikawa, J.R. Choi, M. Fujitsuka, T. Majima, Photoinduced charge-transfer processes on MOF-5 nanoparticles: elucidating differences between metal-organic frameworks and semiconductor metal oxides, J. Phys. Chem. C 112 (2008) 14090–14101.
[15] S. Wang, Q. Yang, F. Chen, J. Sun, K. Luo, F. Yao, X. Wang, D. Wang, X. Li, G. Zeng, Photocatalytic degradation of perfluorooctanoic acid and perfluorooctane sulfonate in water: a critical review, Chem. Eng. J. (2017).
[16] Y. Bai, Y. Dou, L.-H. Xie, W. Rutledge, J.-R. Li, H.-C. Zhou, ChemInform abstract: Zr-based metal-organic frameworks: design, synthesis, structure, and applications, Chem. Soc. Rev. 45 (2016) 2327.
[17] S.J. Garibay, S.M. Cohen, Isoreticular synthesis and modification of frameworks with the UiO-66 topology, Chem. Commun. 46 (2010) 7700–7702.
[18] L. Jiang, X. Yuan, G. Zeng, Z. Wu, J. Liang, X. Chen, L. Leng, H. Wang, H. Wang, Metal-free efficient photocatalyst for stable visible-light photocatalytic degradation of refractory pollutant, Appl. Catal. B (2017).
[19] H. Wang, X. Yuan, Y. Wu, G. Zeng, X. Chen, L. Leng, H. Li, Synthesis and applications of novel graphitic carbon nitride/metal-organic frameworks mesoporous photocatalyst for dyes removal, Appl. Catal. B Environ. s 174–175 (2015) 445–454.
[20] Z. Sha, H.S. Chan, J. Wu, Ag_2CO_3/UiO-66(Zr) composite with enhanced visible-light promoted photocatalytic activity for dye degradation, J. Hazard. Mater. 299 (2015) 132–140.
[21] Y. Deng, L. Tang, C. Feng, G. Zeng, J. Wang, Y. Zhou, Y. Liu, B. Peng, H. Feng, Construction of plasmonic Ag modified phosphorous-doped ultrathin g-C_3N_4 nanosheets/$BiVO_4$ photocatalyst with enhanced visible-near-infrared response ability for ciprofloxacin degradation, J. Hazard. Mater. 344 (2017) 758–769.
[22] K. Mrd, M.S. Shafeeyan, R. Aaa, D. Wmaw, Application of doped photocatalysts for organic pollutant degradation – a review, J. Environ. Manage. 198 (2017) 78.
[23] Z. Wu, X. Yuan, G. Zeng, L. Jiang, H. Zhong, Y. Xie, H. Wang, X. Chen, H. Wang, Highly efficient photocatalytic activity and mechanism of Yb^{3+}/Tm^{3+} codoped In_2S_3 from ultraviolet to near infrared light towards chromium (VI) reduction and rhodamine B oxydative degradation, Appl. Catal. B 225 (2018) 8–21.
[24] L. Jiang, X. Yuan, Y. Pan, J. Liang, G. Zeng, Z. Wu, H. Wang, Doping of graphitic carbon nitride for photocatalysis: a reveiw, Appl. Catal. B 217 (2017) 388–406.
[25] S. Shen, J. Chen, R.T. Koodali, Y. Hu, Q. Xiao, J. Zhou, X. Wang, L. Guo, Activation of MCM-41 mesoporous silica by transition-metal incorporation for photocatalytic hydrogen production, Appl. Catal. B 150–151 (2014) 138–146.
[26] X. Xu, R. Liu, Y. Cui, X. Liang, C. Lei, S. Meng, Y. Ma, Z. Lei, Z. Yang, PANI/FeUiO-66 nanohybrids with enhanced visible-light promoted photocatalytic activity for the selectively aerobic oxidation of aromatic alcohols, Appl. Catal. B 210 (2017) 484–494.
[27] L. Kumaresan, A. Prabhu, M. Palanichamy, E. Arumugam, V. Murugesan, Synthesis and characterization of Zr^{4+}, La^{3+} and Ce^{3+} doped mesoporous TiO_2: evaluation of their photocatalytic activity, J. Hazard. Mater. 186 (2011) 1183–1192.
[28] R. Lin, L. Shen, Z. Ren, W. Wu, Y. Tan, H. Fu, J. Zhang, L. Wu, Enhanced photocatalytic hydrogen production activity via dual modification of MOF and reduced graphene oxide on CdS, Chem. Commun. 50 (2014) 8533.
[29] J. Xu, S. He, H. Zhang, J. Huang, H. Lin, X. Wang, J. Long, Layered metal–organic framework/graphene nanoarchitectures for organic photosynthesis under visible light, J. Mater. Chem. A 3 (2015) 24261–24271.
[30] Z. Yang, X. Xu, X. Liang, C. Lei, L. Gao, R. Hao, D. Lu, Z. Lei, Fabrication of Ce doped UiO-66/graphene nanocomposites with enhanced visible light driven photoactivity for reduction of nitroaromatic compounds, Appl. Surf. Sci. 420 (2017).
[31] C.Y. Wang, Y.J. Zhang, W.K. Wang, D.N. Pei, G.X. Huang, J.J. Chen, X. Zhang, H.Q. Yu, Enhanced photocatalytic degradation of bisphenol A by Co-doped BiOCl nanosheets under visible light irradiation, Appl. Catal. B (2017).
[32] Z. Ding, X. Chen, M. Antonietti, X. Wang, Synthesis of transition metal-modified carbon nitride polymers for selective hydrocarbon oxidation, Chemsuschem 4 (2011) 274.
[33] N.T.T. Ha, O.V. Lefedova, N.N. Ha, Theoretical study on the adsorption of carbon dioxide on individual and alkali-metal doped MOF-5s, Russ. J. Phys. Chem. A 90 (2016) 220–225.
[34] M. Ramezanzadeh, M. Asghari, B. Ramezanzadeh, G. Bahlakeh, Fabrication of an efficient system for Zn ions removal from industrial wastewater based on graphene oxide nanosheets decorated with highly crystalline polyaniline nanofibers (GO-PANI): Experimental and ab initio quantum mechanics approaches, Chem. Eng. J. (2017).
[35] D.A. Almasri, T. Rhadfi, M.A. Atieh, G. Mckay, S. Ahzi, High performance hydroxyiron modified montmorillonite nanoclay adsorbent for arsenite removal, Chem. Eng. J. 335 (2017).
[36] C. Lei, X. Zhu, B. Zhu, C. Jiang, L. Yao, J. Yu, Superb adsorption capacity of hierarchical calcined Ni/Mg/Al layered double hydroxides for Congo red and Cr(VI) ions, J. Hazard. Mater. 321 (2017) 801–811.
[37] W. Hou, X. Yuan, W. Yan, G. Zeng, H. Dong, X. Chen, L. Leng, Z. Wu, L. Peng, In situ synthesis of In_2S_3@MIL-125(Ti) core-shell microparticle for the removal of

tetracycline from wastewater by integrated adsorption and visible-light-driven photocatalysis, Appl. Catal. B 186 (2016) 19–29.
[38] M. Oveisi, M.A. Asli, N.M. Mahmoodi, MIL-Ti metal-organic frameworks (MOFs) nanomaterials as superior adsorbents: Synthesis and ultrasound-aided dye adsorption from multicomponent wastewater systems, J. Hazard. Mater. 347 (2018) 123–140.
[39] S. Panneri, M. Thomas, P. Ganguly, B.N. Nair, A.P. Mohamed, K.G.K. Warrier, U.S. Hareesh, C_3N_4 anchored ZIF-8 composites: photo-regenerable, high capacity sorbents as adsorptive photocatalysts for the effective removal of tetracycline from water, Catal. Sci. Technol. 7 (2017).
[40] J. Abdi, M. Vossoughi, N.M. Mahmoodi, I. Alemzadeh, Synthesis of metal-organic framework hybrid nanocomposites based on GO and CNT with high adsorption capacity for dye removal, Chem. Eng. J. 326 (2017) 1145–1158.
[41] P. Wang, L. Tang, X. Wei, G. Zeng, Y. Zhou, Y. Deng, J. Wang, Z. Xie, W. Fang, Synthesis and application of iron and zinc doped biochar for removal of p-nitrophenol in wastewater and assessment of the influence of co-existed Pb(II), Appl. Surf. Sci. 392 (2017) 391–401.
[42] Z. Wu, H. Zhong, X. Yuan, H. Wang, L. Wang, X. Chen, G. Zeng, Y. Wu, Adsorptive removal of methylene blue by rhamnolipid-functionalized graphene oxide from wastewater, Water Res. 67 (2014) 330–344.
[43] Q. Song, Y. Fang, Z. Liu, L. Li, Y. Wang, J. Liang, Y. Huang, J. Lin, L. Hu, J. Zhang, The performance of porous hexagonal BN in high adsorption capacity towards antibiotics pollutants from aqueous solution, Chem. Eng. J. (2017).
[44] Z. Zhou, Y.G. Liu, S.B. Liu, H.Y. Liu, G.M. Zeng, X.F. Tan, C.P. Yang, Y. Ding, Z.L. Yan, X.X. Cai, Sorption performance and mechanisms of arsenic(V) removal by magnetic gelatin-modified biochar, Chem. Eng. J. 314 (2017) 223–231.
[45] Y. Yan, Q. An, Z. Xiao, W. Zheng, S. Zhai, Flexible core-shell/bead-like alginate@PEI with exceptional adsorption capacity, recycling performance toward batch and column sorption of Cr(VI), Chem. Eng. J. 313 (2017) 475–486.
[46] L. Tang, J. Yu, Y. Pang, G. Zeng, Y. Deng, J. Wang, X. Ren, S. Ye, B. Peng, H. Feng, Sustainable efficient adsorbent: Alkali-acid modified magnetic biochar derived from sewage sludge for aqueous organic contaminant removal, Chem. Eng. J. 336 (2018) 160–169.
[47] J. Li, K. Zhao, Y. Yu, L. Zhang, Facet-level mechanistic insights into general homogeneous carbon doping for enhanced solar-to-hydrogen conversion, Adv. Funct. Mater. 25 (2015) 2189–2201.
[48] Y. Boyjoo, H. Sun, J. Liu, V.K. Pareek, S. Wang, A review on photocatalysis for air treatment: From catalyst development to reactor design, Chem. Eng. J. (2016).
[49] Q. Liang, M. Zhang, Z. Zhang, C. Liu, S. Xu, Z. Li, Zinc phthalocyanine coupled with UiO-66 (NH_2) via a facile condensation process for enhanced visible-light-driven photocatalysis, J. Alloy. Compd. 690 (2017) 123–130.
[50] Z. Guan, G. Kim, W. Choi, Visible light driven photocatalysis mediated via ligand-to-metal charge transfer (LMCT): an alternative approach to solar activation of titania, Energy Environ. Sci. 7 (2014) 954–966.
[51] A. Šutka, T. Käämbre, R. Pärna, I. Juhnevica, M. Maiorov, U. Joost, V. Kisand, Co doped ZnO nanowires as visible light photocatalysts, Solid State Sci. 56 (2016) 54–62.
[52] Y. Fu, L. Sun, H. Yang, L. Xu, F. Zhang, W. Zhu, Visible-light-induced aerobic photocatalytic oxidation of aromatic alcohols to aldehydes over Ni-doped NH_2-MIL-125(Ti), Appl. Catal. B 187 (2016) 212–217.
[53] Z.J. Xie, Y.P. Feng, F.L. Wang, D.N. Chen, Q.X. Zhang, Y.Q. Zeng, W.Y. Lv, G.G. Liu, Construction of carbon dots modified MoO_3/g-C_3N_4 Z-scheme photocatalyst with enhanced visible-light photocatalytic activity for the degradation of tetracycline, Appl. Catal. B-Environ. 229 (2018) 96–104.
[54] H. Dong, Z. Jiang, C. Zhang, J. Deng, K. Hou, Y. Cheng, L. Zhang, G. Zeng, Removal of tetracycline by Fe/Ni bimetallic nanoparticles in aqueous solution, J Colloid Interface Sci 513 (2018) 117–125.
[55] C. Fei, Y. Qi, Z. Yu, H. An, J. Zhao, T. Xie, Q. Xu, X. Li, D. Wang, G. Zeng, Photoreduction of bromate in drinking water by metallic Ag and reduced graphene oxide (RGO) jointly modified $BiVO_4$ under visible light irradiation, Water Res. 101 (2016) 555–563.
[56] B. Huang, Y. Liu, B. Li, S. Liu, G. Zeng, Z. Zeng, X. Wang, Q. Ning, B. Zheng, C. Yang, Effect of Cu(II) ions on the enhancement of tetracycline adsorption by Fe_3O_4@SiO_2-Chitosan/Graphene oxide nanocomposite, Carbohydr. Polym. 157 (2017) 576.
[57] N. Tian, Q.M. Jia, H.Y. Su, Y.F. Zhi, A.H. Ma, J. Wu, S.Y. Shan, The synthesis of mesostructured NH_2-MIL-101(Cr) and kinetic and thermodynamic study in tetracycline aqueous solutions, J. Porous Mater. 23 (2016) 1–10.
[58] A. Takdastan, A.H. Mahvi, E.C. Lima, M. Shirmardi, A.A. Babaei, G. Goudarzi, A. Neisi, F.M. Heidari, M. Vosoughi, Preparation, characterization, and application of activated carbon from low-cost material for the adsorption of tetracycline antibiotic from aqueous solutions, Water Sci. Technol. J. Int. Assoc. Water Pollut. Res. 74 (2016) 2349.
[59] Y. Shi, Z. Yang, B. Wang, H. An, Z. Chen, H. Cui, Adsorption and photocatalytic degradation of tetracycline hydrochloride using a palygorskite-supported Cu_2O–TiO_2 composite, Appl. Clay Sci. 119 (2016) 311–320.
[60] S. Álvarez-Torrellas, R.S. Ribeiro, H.T. Gomes, G. Ovejero, J. García, Removal of antibiotic compounds by adsorption using glycerol-based carbon materials, Chem. Eng. J. 296 (2016) 277–288.
[61] T. Hu, H. Lv, S. Shan, Q. Jia, H. Su, N. Tian, S. He, Porous structured MIL-101 synthesized with different mineralizers for adsorptive removal of oxytetracycline from aqueous solution, RSC Adv. 6 (2016).
[62] C. Chen, D. Chen, S. Xie, H. Quan, X. Luo, L. Guo, Adsorption behaviors of organic micropollutants on zirconium metal-organic framework UiO-66: analysis of surface interactions, ACS Appl. Mater Interfaces 9 (2017) 41043–41054.
[63] C.S. Wu, Z.H. Xiong, C. Li, J.M. Zhang, Zeolitic imidazolate metal organic framework ZIF-8 with ultra-high adsorption capacity bound tetracycline in aqueous solution, Rsc Adv. 5 (2015) 82127–82137.